

Solving decision problems with endogenous uncertainty and conditional information revelation using influence diagrams

Olli Herrala^a, Tommi Ekhholm^b, Fabricio Oliveira^{a,*}

^a*Department of Mathematics and Systems Analysis, Aalto University, School of Science, FI-00076 Aalto, Finland*

^b*Finnish Meteorological Institute, Helsinki, Finland*

Abstract

Despite methodological advances for modeling decision problems under uncertainty, representing endogenous uncertainty still proves challenging both in terms of modeling capabilities and computational requirements. A novel reformulation based on rooted junction trees (RJTs) provides an approach for solving such decision problems using off-the-shelf mathematical optimization solvers. This is made possible by using an influence diagram to represent a given decision problem and reformulating it as an RJT, which is then represented as a mixed-integer linear programming model.

In this paper, we focus on the type of endogenous uncertainty that received less attention in the rooted junction tree approach: conditionally observed information. Multi-stage stochastic programming models use conditional non-anticipativity constraints to represent such uncertainties, and we show how such constraints can be incorporated into RJT formulations. This allows us to consider the two main types of endogenous uncertainty simultaneously, namely decision-dependent information structure and decision-dependent probability distribution. Finally, the extended framework is illustrated with a large-scale cost-benefit problem regarding climate change mitigation.

Keywords: endogenous uncertainty, stochastic programming, junction trees, climate change mitigation

*Corresponding author: fabricio.oliveira@aalto.fi

1. Introduction

Stochastic programming (SP) is one of the most widespread mathematical programming-based frameworks for decision-making under uncertainty. In general, SP casts decision problems subject to parametric uncertainty as deterministic equivalents in the form of large-scale linear or mixed-integer linear programming (LP/MILP) models that can be solved with standard optimization techniques. A common assumption in SP models is that the stochastic processes, particularly the state probabilities and/or observed values, are not influenced by the previously made decisions. The uncertainty is thus *exogenous*. This is methodologically convenient, for the deterministic equivalent model has the same nature as its stochastic counterpart, retaining important characteristics such as linearity, or more generally, convexity.

In this paper, we focus on a much less explored class of stochastic problems presenting *endogenous* uncertainty. In this more general setting, the decisions made at previous stages can affect the uncertainty faced in later stages. It is common to classify these problems according to the nature of the endogenous structure arising in the decision problem. Hellemo et al. (2018) propose a taxonomy of such problems, classifying the endogenous uncertainties into two distinct types. In Type 1 problems, earlier decisions influence the later events' probability distribution (i.e., realizations and/or the probabilities associated with each realization). For example, deciding to perform maintenance on a car engine influences the probability of it breaking in the future. In Type 2 problems, the *information structure* is influenced by the decision-making. Continuing with the car example, deciding to inspect the engine does not affect the probability of it breaking, but provides information that enables a better-informed maintenance decision. Hellemo et al. (2018) also introduce Type 3, which combines the Type 1 and Type 2 endogenous uncertainties.

Overall, solving SP problems with endogenous uncertainty is difficult, with Type 1 requiring specific uncertainty structures (Hellemo et al., 2018) and Type 2 resulting in computationally burdensome mixed-integer models (Apap and Grossmann, 2017). In contrast, the field of decision analysis tackles Type 1 endogenous uncertainty using influence diagrams, and Parmentier et al. (2020) utilize these ideas by first reformulating the diagram into a rooted junction tree (RJT). This RJT is then further converted to a mixed-integer linear programming (MILP) model, for which powerful off-the-shelf solvers exist. The intermediate step is not strictly necessary, as Salo et al. (2022) present an alternative formulation directly converting the influence diagram into a MILP. However, as discussed in Herrala et al. (2023), the RJT formulation generally results in better computational performance.

Prior research on influence diagram models focuses more prominently on Type 1 endogenous uncertainties. A relevant exception is Salo et al. (2022), who presented a simple problem incorporating Type 2 endogenous uncertainty in the influence diagram using their Decision Programming framework. However, their discussion regarding this class of endogenous uncertainty is only superficial and lacks an analysis of the implications associated with its modeling as proposed. Aiming to fill this lacuna, our paper explores the possibility of modeling Type 2 endogenous uncertainty within the resulting MILP model by implementing conditional non-anticipativity constraints (Apap and Grossmann, 2017), which were originally conceived to be used in multistage stochastic programming.

It should be noted that these constraints, as presented in the literature, require that a scenario tree structure is embedded within the model formulation since they effectively connect decisions across branches of the scenario tree. While the influence diagram models we employ do not use a scenario tree representation of the problem, we show that these constraints can be adapted into the model proposed by Parmentier et al. (2020). In doing so, we show how the RJT formulation can be enhanced to become a suitable framework for T3ESP problems comprising both Type 1 and 2 endogenous uncertainties, while still retaining prior computationally favorable properties of the mathematical model such as linearity, convexity and the ability to incorporate, e.g., chance constraints (Herrala et al., 2023).

The formulation presented in Parmentier et al. (2020) accommodates only discrete decisions, and Salo et al. (2022) acknowledge the limitations of using influence diagram-based models for problems involving continuous decisions, a challenge discussed in more detail in Bielza et al. (2011). Decisions such as order or production quantities and investment amounts arise in various problem settings, and we show that these decision spaces can be approximated with discrete sets of alternatives, at the expense of trading off solution quality and computational performance. To circumvent this issue, we show that if the problem has a separable structure, the submodel-tree decomposition proposed in Lee et al. (2021) can be employed, making it possible to incorporate continuous decisions, as long as they do not affect the endogenous probabilities in the model. In our computational experiments, the solution times using this decomposition are similar to those using a very coarse discretization of the decision space. In the illustrative climate change cost-benefit analysis case study that originally motivated our developments, we consider uncertain climate parameters and technological progress and the problem of determining the optimal strategy for climate and technology research, as well as the optimal emission levels for 2030-2070.

This paper is structured as follows. In Section 2, we present an overview of multi-stage stochastic programming and the formulation in Parmentier et al. (2020). In Section 3, our methodological contributions are described in detail, starting from conditionally observed information and continuing with the role of subdiagram decomposition in incorporating continuous variables. The computational performance of these contributions is then assessed in Section 4. In Section 5 we illustrate the use of the framework by considering a larger-scale problem of climate change cost-benefit analysis. Section 6 concludes and provides directions for further development.

2. Modeling problems with endogenous and exogenous uncertainties

2.1. Decision-making under endogenous uncertainty

Solution approaches for multi-stage stochastic programming (MSSP) are often based on formulating the deterministic equivalent problem using a scenario tree, as described in, e.g., Ruszczyński (1997). A scenario tree represents the structure of the uncertain decision process, and non-anticipativity constraints (NACs) (Rockafellar and Wets, 1991) are employed to enforce the information structure in the formulation. NACs state that a decision must be the same for two scenarios if those scenarios are indistinguishable when making the decision.

In endogenously uncertain problems, the decisions can affect the timing, event probabilities, or outcomes of uncertain events further in the process. As previously discussed, endogenous uncertainty is often divided into *decision-dependent probabilities* (Type 1) and *decision-dependent information structure* (Type 2) (Hellemo et al., 2018). In this context, information structure often refers to when the realization of each uncertain event is observed, if ever. In contrast, exogenously uncertain problems have a fixed information structure with the timing of observations known a priori.

Type 2 uncertainty has been more widely addressed in the SP literature, perhaps due to one of its subclasses having a strong connection to exogenously uncertain problems. In the taxonomy presented in Hellemo et al. (2018), this specific type of endogenous uncertainty is called conditional information revelation. For the sake of terminology consistency, we refer to this as *conditionally observed information*. In this subclass, the decisions only affect the time at which the (exogenous) uncertainty is revealed to the decision maker. One of the earliest publications on such uncertainty is Jonsbråten et al. (1998), where the authors describe a branching algorithm for solving a subcontracting problem. Goel and Grossmann (2006) consider a process network problem where the yield of a new process is uncertain prior to installation. Other applications include open pit mining (Boland et al., 2008), clinical trial planning for drug development (Colvin and Maravelias, 2010) and technology project portfolio management (Solak et al., 2008).

Similar solution methods are employed in problems with exogenous uncertainty and conditionally observed information. The main difference is that conditional observation requires the use of *conditional non-anticipativity constraints* (C-NACs), as the distinguishability between scenarios at any given stage is dependent on earlier decisions. This conditional dependency results in disjunctive constraints that require specific reformulation techniques (Apap and Grossmann, 2017). The main challenge arising from this approach is that the number of constraints rapidly increases with problem size, resulting in computational intractability for large problems. Apap and Grossmann (2017) also propose omitting redundant constraints, in an attempt to mitigate the tractability issues. In their example considering a production planning problem, this results in roughly a 99% decrease in the problem size. Despite these substantial improvements, the reduced model is still considerably large and cannot be solved to the optimum within a reasonable computation time under their experimental setting, illustrating how challenging such problems are.

Type 1 endogenous uncertainty is more challenging from a mathematical modeling standpoint because the uncertain events depend on earlier decisions. Consequently, a scenario tree-based representation cannot be posed, as the scenario probabilities in a scenario tree cannot depend on decisions. Therefore, the well-established solution techniques for MSSP cannot be directly applied to these problems. Despite these challenges, some discussion on Type 1 endogenous uncertainty is found in the literature. Peeta et al. (2010) discuss the fortification of a structure in a network, where the probability of failure depends on the fortification decision. Dupačová (2006) presents a summary of problems with Type 1 uncertainties and Escudero et al. (2020) present solution approaches to multi-stage problems where the first-stage decisions influence the scenario probabilities in later stages. Examples of such problems can be found in Zhou et al. (2022) and Li and Liu (2023). Finally, reformulations and custom algorithms for various Type 1 problems are further summarized in Hellemo et al. (2018). However, these approaches assume specific relationships between decisions and probabilities and result in non-convex nonlinear formulations. Consequently, these approaches are not easily generalizable to different problems.

From a perspective other than stochastic programming, Lauritzen and Nilsson (2001) present the “pig farm problem”, where the health of a pig depends on the treatment decisions, introducing the concept of limited memory influence diagrams (LIMID), thus relaxing the no-forgetting assumption in influence diagrams. The no-forgetting assumption states that when making a decision, all prior decisions and outcomes of uncertain events are known. This assumption results in significant limitations for distributed decision-making and leads to computational challenges in multi-period problems where the decisions later in the process are conditional on the full history of the problem.

2.2. Influence diagrams

An *influence diagram* $G_{ID} = (N, A_{ID})$ is an acyclic graph formed by nodes $j \in N = N^C \cup N^D \cup N^V$ and arcs $a \in A_{ID} = \{(i, j) \mid i, j \in N\}$ ¹. Nodes N^C and N^D are the sets of chance and decision nodes, respectively, and N^V is a collection of value nodes representing the consequences incurred from the decisions made at nodes N^D and the chance events realized at nodes N^C . In Fig. 1, the decision nodes are represented by squares, the chance nodes by circles, and the value nodes by diamonds.

Each decision and chance node $j \in N^C \cup N^D$ can assume a state s_j from a discrete and finite set of states S_j . For a decision node $j \in N^D$, S_j represents the available choices; for a chance node $j \in N^C$, S_j is the set of possible realizations. The arcs (i, j) in $A_{ID} = \{(i, j) \mid i, j \in N\}$ represent influence between nodes. In Fig. 1, the arcs are represented by arrows between

¹We use the subscript *ID* for G_{ID} and A_{ID} to distinguish between influence diagrams and rooted junction trees. Rooted junction trees are described in Section 2.3.

the nodes. Before defining this notion of influence further, let us first define a few necessary concepts.

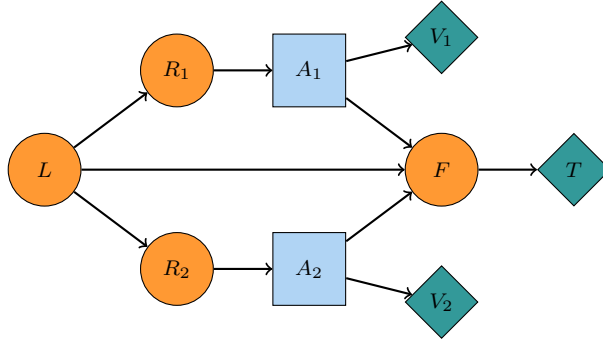


Figure 1: An influence diagram representation of a decision problem

The *information set* comprises the immediate predecessors of a given node $j \in N$ and is defined as $I(j) = \{i \in N \mid (i, j) \in A_{ID}\}$. In the graphical representation, this corresponds to the set of nodes that have an arrow pointing directly to node j . For example, in Fig. 1, the information set of F consists of L , A_1 and A_2 . The decision $s_j \in S_j$ made in each decision node $j \in N^D$ and the conditional probabilities of the states $s_j \in S_j$ in each chance node $j \in N^C$ depend on their *information state* $s_{I(j)} \in S_{I(j)}$, where $S_{I(j)} = \prod_{i \in I(j)} S_i$. Referring to our example, the probabilities of different outcomes in F are conditional on the decisions in A_1 and A_2 and the random outcome in L . Let us define $X_j \in S_j$ as the realized state at a chance node $j \in N^C$. Using the notion of information states, the conditional probability of observing a given state s_j for $j \in N^C$ is $\mathbb{P}(X_j = s_j \mid X_{I(j)} = s_{I(j)})$.

For a decision node $j \in N^D$, let $Z_j : S_{I(j)} \rightarrow S_j$ be a mapping between each information state $s_{I(j)} \in S_{I(j)}$ and decision $s_j \in S_j$. That is, $Z_j(s_{I(j)})$ defines a *local decision strategy*, which represents the choice of some $s_j \in S_j$ in $j \in N^D$, given the information $s_{I(j)}$. Note that we do not consider mixed strategies, where each information state would be mapped to an arbitrary probability distribution over S_j . Instead, we only consider deterministic strategies that can be represented by an indicator function $\mathbb{I} : S_{I(j)} \times S_j \rightarrow \{0, 1\}$ defined so that

$$\mathbb{I}(s_{I(j)}, s_j) = \begin{cases} 1, & \text{if } Z_j \text{ maps } s_{I(j)} \text{ to } s_j, \text{ i.e., } Z_j(s_{I(j)}) = s_j; \\ 0, & \text{otherwise.} \end{cases} \quad (1)$$

A (global) decision strategy is the collection of local decision strategies in all decision nodes: $Z = (Z_j)_{j \in N^D}$, selected from the set of all possible strategies \mathbb{Z} .

At each value node $v \in N^V$, a real-valued utility function $U_v : S_{I(v)} \rightarrow \mathbb{R}$ maps the information state $s_{I(v)}$ of v to a utility value U_v . The default objective is to maximize the expected utility of a strategy, but other objectives such as conditional Value-at-Risk can also be used (Salo et al., 2022; Herrala et al., 2023).

2.3. Rooted junction trees

As shown in Salo et al. (2022), it is possible to obtain a mixed-integer linear programming (MILP) model directly from the influence diagram representation of the problem. However, the authors observe that the model size increases exponentially with the number of nodes, resulting in computational challenges with relatively small problems. To mitigate this exponential growth, Parmentier et al. (2020) proposes first reformulating the influence diagram into a *rooted junction tree* (RJT) $G_{RJT} = (V, A_{RJT})$, a directed graph consisting of clusters $C \in V$ of nodes $j \in N$, and arcs between these clusters, with the underlying undirected graph (obtained by replacing the directed edges A_{RJT} with undirected edges) being a tree. The core idea of the RJT reformulation

is to construct the joint probability distributions corresponding to each cluster, which results in a smaller MIP model compared to the path-based approach in Salo et al. (2022). The computational performance of the RJT reformulation is compared to Decision Programming (Salo et al., 2022) in Herrala et al. (2023), where the authors show that the growth in model size as more nodes are introduced to the diagram is significantly slower in RJT models.

The first important property of an RJT is the *running intersection property*, i.e., if a node $j \in N$ is in two clusters of the tree, it is also in all clusters on the (undirected) path between these clusters. From this property, it follows that the subgraph of G_{RJT} induced by a node j (formed by clusters $C \in V$ for which $j \in C$, and the arcs connecting such clusters) is a rooted tree. For example, in Fig. 2, the node A_1 appears in four clusters that form a rooted tree.

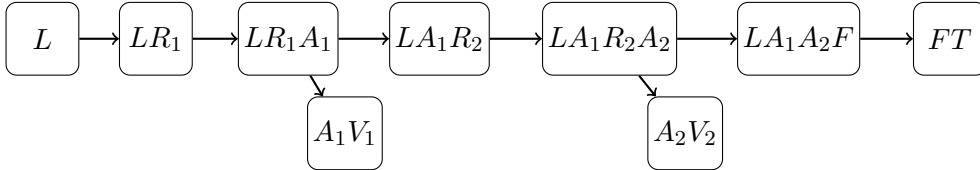


Figure 2: A gradual RJT representation of the ID in Fig. 1

More specifically, Parmentier et al. (2020) consider gradual RJTs, where each cluster is the *root cluster* of exactly one node $j \in N$, and the root cluster of node j is denoted with C_j . A root cluster is defined as the root of the subgraph of the RJT induced by a node j . For example, the root cluster of the subtree induced by A_1 is denoted as C_{A_1} . Finally, it is required that $I(j) \subset C_j$ for all $j \in N$. These properties result in a convenient structure where for each pair of adjacent clusters $(C_i, C_j) \in A_{RJT}$, we have $C_j \setminus C_i = j$, and the joint probability distribution of all nodes in C_j can thus always be obtained from the probability distribution of C_i and the conditional probability $\mathbb{P}(X_j = s_j \mid X_{I(j)} = s_{I(j)})$ using the chain rule. As will be described next, this allows the problem to be formulated as a mixed-integer programming (MIP) model, which allows for employing standard techniques widely available in off-the-shelf solvers.

While any gradual RJT fulfilling these requirements can be used to formulate the MIP model (2)-(8), large clusters result in larger models and the associated computational challenges. To avoid forming RJTs possessing large clusters, Parmentier et al. (2020) present two algorithms for converting a LIMID into an RJT with minimal clusters. In summary, both algorithms build the RJT by traversing the LIMID according to a reverse topological order, adding a cluster corresponding to one of the nodes in the diagram, and the necessary arcs from this cluster to previously introduced clusters, repeating until the RJT has been built. The first algorithm uses a given topological ordering, while the second also forms a topological ordering resulting in smaller clusters. For a more detailed description of the properties of gradual RJTs, we refer the reader to Parmentier et al. (2020) and Herrala et al. (2023).

Let us define the binary variable $z(s_j \mid s_{I(j)})$ that takes value 1 if $Z_j(s_{I(j)}) = s_j$, and 0 otherwise, for all $j \in N^D$, $s_j \in S_j$, and $s_{I(j)} \in S_{I(j)}$. These variables correspond to the indicator function (1), representing local decision strategies at each decision node $j \in N^D$. Additionally, we define variables $\mu_{C_j} \geq 0$ representing the joint probability distribution of nodes $i \in C_j$. The expected utility maximization problem corresponding to the gradual RJT can then be

formulated as

$$\max \sum_{j \in N^V} \sum_{s_{C_j} \in S_{C_j}} \mu_{C_j}(s_{C_j}) u_{C_j}(s_{C_j}) \quad (2)$$

$$\text{s.t.} \quad \sum_{s_{C_j} \in S_{C_j}} \mu_{C_j}(s_{C_j}) = 1, \quad \forall j \in N \quad (3)$$

$$\sum_{\substack{s_{C_i} \in S_{C_i}, \\ s_{C_i \cap C_j} = s_{C_i \cap C_j}^*}} \mu_{C_i}(s_{C_i}) = \sum_{\substack{s_{C_j} \in S_{C_j}, \\ s_{C_i \cap C_j} = s_{C_i \cap C_j}^*}} \mu_{C_j}(s_{C_j}), \quad \forall (C_i, C_j) \in A_{RJT}, s_{C_i \cap C_j}^* \in S_{C_i \cap C_j} \quad (4)$$

$$\mu_{C_j}(s_{C_j}) = \mu_{\bar{C}_j}(s_{\bar{C}_j}) \mathbb{P}(X_j = s_j \mid X_{I(j)} = s_{I(j)}), \quad \forall j \in N^C \cup N^V, s_{C_j} \in S_{C_j} \quad (5)$$

$$\mu_{C_j}(s_{C_j}) = \mu_{\bar{C}_j}(s_{\bar{C}_j}) z(s_j \mid s_{I(j)}), \quad \forall j \in N^D, s_{C_j} \in S_{C_j} \quad (6)$$

$$\mu_{C_j}(s_{C_j}) \geq 0, \quad \forall j \in N, s_{C_j} \in S_{C_j} \quad (7)$$

$$z(s_j \mid s_{I(j)}) \in \{0, 1\}, \quad \forall j \in N^D, s_j \in S_j, s_{I(j)} \in S_{I(j)}. \quad (8)$$

The objective function (2) is the expected utility associated with the strategy $Z \in \mathbb{Z}$ represented by the decision variables z . Following the definition of a gradual RJT, $I(j) \subset C_j$ and there is exactly one cluster corresponding to each value node $j \in N^V$. We thus set utility values associated with these clusters to $u_{C_j}(s_{C_j}) = U_j(s_{I(j)})$ using the utility function defined in Section 2.2. Constraints (3) and (7) state that the decision variables μ_{C_j} must represent valid probability distributions, i.e., have nonzero probabilities that sum to one, and constraint (4) enforces local consistency between adjacent clusters. Here, local consistency means that the distribution $\mu_{C_i \cap C_j}$ must be the same when obtained as a marginal distribution from C_i or C_j . The states of the nodes in the intersection of clusters C_i and C_j are denoted with $s_{C_i \cap C_j}$, and a specific state combination in this set is denoted with $s_{C_i \cap C_j}^*$.

Constraints (5) and (6) propagate the probability information in the junction tree using the chain rule $\mathbb{P}(X, Y) = \mathbb{P}(Y) \mathbb{P}(X|Y)$. For notational brevity, we use $\bar{C}_j = C_j \setminus j$, for which $\mu_{\bar{C}_j}(s_{\bar{C}_j}) = \sum_{s_j} \mu_{C_j}(s_{C_j})$. Combined with the local consistency constraints (4), this ensures that $\mu_{\bar{C}_j}$ can be used in the chain rule to obtain μ_{C_j} . It should be noted that while constraint (6) contains a product of two decision variables, the decision strategy variables z are binary, making (6) an indicator constraint. This allows one to linearize the product using methods discussed in, e.g., Mitra et al. (1994), and the problem can be considered an instance of mixed integer linear programming (MILP).

As an example, we discuss the variables and constraints for the first four clusters in Fig. 2. For completeness, the corresponding parts of the model are presented in Appendix C. For the first cluster, we introduce variables $\mu_{C_L} \geq 0$ and add a constraint $\sum_{s_L \in S_L} \mu_{C_L}(s_L) = 1$. As there is only one node in the cluster, constraint (5) becomes simply $\mu_{C_L}(s_L) = \mathbb{P}(X_L = s_L)$, that is, the probability distribution of the one-node root cluster must match the given distribution for that node. For the next cluster, we define $\mu_{C_{R_1}}$ in a similar way, but constraint (5) now becomes $\mu_{C_{R_1}}(s_L, s_{R_1}) = \mu_{\bar{C}_{R_1}}(s_L) \mathbb{P}(X_{R_1} = s_{R_1} \mid X_L = s_L)$, where $\mu_{\bar{C}_{R_1}}(s_L) = \mu_{C_L}(s_L)$ in this case, as $C_{R_1} \setminus R_1 = \{L\} = C_L$. Finally, the intersection $C_L \cap C_{R_1}$ is L and constraint (4) states that for each $s_L^* \in S_L$, we must have $\mu_{C_L}(s_L^*) = \sum_{s_{R_1}} \mu_{C_{R_1}}(s_L^*, s_{R_1})$.

The process is otherwise the same for the second and third clusters, but for the third cluster, constraint (6) is used instead of (5). For the fourth cluster C_{V_1} , we notice that \bar{C}_{V_1} is not equal to the parent cluster C_{A_1} . Instead, constraint (4) enforces local consistency and the distribution \bar{C}_{V_1} is therefore effectively defined using the parent cluster distribution. Finally, as $V_1 \in N^V$ is a value node, this cluster contributes $\sum_{s_{A_1} \in S_{A_1}, s_{V_1} \in S_{V_1}} \mu_{C_{V_1}}(s_{A_1}, s_{V_1}) u_{V_1}(s_{A_1}, s_{V_1})$ to the objective function.

3. Methodological developments

3.1. Conditionally observed information

As originally proposed, the approaches to formulate influence diagrams as MILP models most prominently focus on problems with Type 1 endogenous uncertainty, i.e., decision-dependent probabilities. However, many MSSP problems involve conditionally observed information and being able to model this within influence diagrams would make the models more generally applicable.

The previously discussed influence diagram in Fig. 1 represents the so-called N-monitoring problem (Salo et al., 2022), where a single underlying variable L is observed by N independent decision makers (in Fig. 1, $N = 2$) through reports represented by R_i . This version of the model assumes that the reports are always available, but in reality, these reports might have a cost associated with their acquisition. Consequently, the cost may be higher than the value gained from the report and the optimal solution would thus be not to pay for the report. If we modify the problem so that the decision maker (DM) can choose whether or not to acquire the report, we say that observing the information in the report is conditional on the decision to pay for the report. We refer to this variant as the conditional N-monitoring problem.

A key concept with conditionally observed information is *distinguishability*. The outcome of a report itself, say s_{R_i} or s'_{R_i} , is independent of the DM's choice to procure the report, but can only be observed if the DM pays for the report. Therefore, the DM cannot see the difference between s_{R_i} and s'_{R_i} when making the decision A_i unless the report is procured. Otherwise, the report's outcome is not observed and the states s_{R_i} and s'_{R_i} are indistinguishable at A_i .

Our formulations for conditionally observed information focus on two key elements. First, we have the decisions or random events that the observation is conditional on, which we denote as the *distinguishability set* $T_{i,j} \subset N^C \cup N^D$. Second, the observation depends on a *distinguishability condition* $F_{i,j} : S_{T_{i,j}} \rightarrow \{0, 1\}$. Here, $i \in N^C \cup N^D$ denotes the conditionally observed node and $j \in N^D$ is the decision node where that information is available if the distinguishability condition is fulfilled. Note that both i and $T_{i,j}$ must be contained in the cluster C_j , which can be achieved by treating them as a part of the information set $I(j)$ when converting the ID to an RJT.

In most cases, the conditionally observed node is a chance node, but it can also be a decision node. Such cases might arise in the context of distributed decision-making, where the decisions are made by multiple agents and observing the decision of another agent does not happen automatically, or problems in which previous decisions are not remembered by default and the decision maker must instead pay a price to retrieve information on past decisions. Distributed decision making in the context of influence diagrams is discussed in, e.g., Detwarasiti and Shachter (2005), and Piccione and Rubinstein (1997) point out that decision makers can often affect what they remember by choosing to keep track of information (including decisions) they would otherwise forget.

Using the notion of distinguishability sets and conditions, we can define *conditional arcs*

$$a_c \in A_c = \{(i, j) \mid i \in N^C \cup N^D, j \in N^D, T_{i,j} \neq \emptyset\} \quad (9)$$

to describe conditionally observed information in influence diagrams. Specifically, we say that a conditional arc a_c from node $i \in N^C \cup N^D$ to node $j \in N^D$ is active (i.e., node i is observed when making the decision corresponding to node j) if $F_{i,j}(s_{T_{i,j}}) = 1$. If $T_{i,j}$ is empty, there is no conditional observation of i in j and, thus, no conditional arc between these nodes exists. The concept is illustrated in Fig. 3.

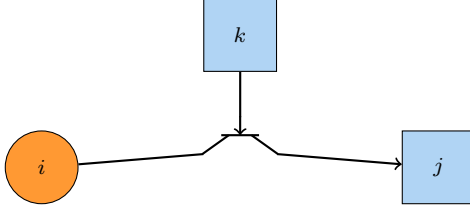


Figure 3: An illustration of a conditional arc (i, j) . Nodes i and j correspond to the earlier notation where the realization of i is conditionally observed in j . The distinguishability set is $T_{i,j} = \{k\}$ and the middle part of the arc represents that the flow of information from i to j is conditional on k .

Using the conditional N-monitoring example, the chance node i in Fig. 3 corresponds to the report (node R_i in Fig. 1), decision node k to the decision on whether or not to acquire the report, and j to node A_i . When making the decision in A_i , the report is available only if the decision maker chooses to acquire the report. Hence, the distinguishability set is $T_{i,j} = \{k\}$, and the distinguishability condition is $F_{i,j}(s_{T_{i,j}}) = \mathbb{I}(s_k = \text{“acquire report”})$, where the indicator function $\mathbb{I}(\cdot)$ is defined as

$$\mathbb{I}(x = x^*) = \begin{cases} 1 \text{ (true)}, & \text{if } x = x^*, \\ 0 \text{ (false)}, & \text{otherwise.} \end{cases}$$

If the distinguishability set includes more than one node, alternative functions $F_{i,j}$ might be employed for modeling the conditional dependencies between the nodes. For example, if there are several projects that reveal the same information in node $i \in N$ and completing any of these projects is sufficient for the information to be revealed, $F_{i,j}(s_{T_{i,j}}) = \bigvee_{k \in T_{i,j}} \mathbb{I}(s_k = s_k^*)$ can be used; or if all of the projects are required for the information revelation, $F_{i,j}(s_{T_{i,j}}) = \bigwedge_{k \in T_{i,j}} \mathbb{I}(s_k = s_k^*)$ is appropriate. An example of such conditions is found in Tarhan et al. (2009), where different uncertainties in oil field development are gradually revealed, and the uncertainty in the amount of recoverable oil in a reservoir can be resolved in two different ways, namely drilling a sufficient number of wells or using the reservoir for production for long enough.

3.2. Incorporating conditionally observed information in rooted junction trees

The conditional arcs are designed to describe conditionally observed information in influence diagrams. However, they are a general representation of the concept, not a modeling solution. In what follows, we present two alternative approaches for incorporating this concept into the RJT models, which ultimately enables solving Type 3 endogenously uncertain stochastic problems. The first approach employs *observation nodes*. These have been used in influence diagram literature, in problems such as the used car buyer problem (Howard and Matheson, 2005) or the oil wildcatter problem (Raiffa, 1968). The second approach utilizes conditional non-anticipativity constraints, which are used in stochastic programming for modeling the decision-dependent information structure. We show that using the mixed-integer reformulation (2)-(8) as an alternative to adding observation nodes to the diagram allows for employing conditional non-anticipativity constraints in modeling and solving limited memory influence diagrams. In Section 4, the computational performance of the two approaches is compared.

3.2.1. Observation nodes

Observation nodes portray how the decision maker observes the information. By enforcing that earlier decisions affect the probability distribution of the observations, Type 2 uncertainty is effectively transformed into Type 1 uncertainty, making it directly amenable to influence diagrams and their associated analysis techniques. This approach is also used in Salo et al. (2022). While observation nodes have been previously used in the literature on influence diagrams, the specific connection between conditionally observed information and observation nodes has

not been explicitly discussed nor has the computational impact of incorporating conditional information been assessed.

In effect, each conditional arc is replaced with an observation node, as illustrated in Fig. 4. The information set of the observation node is the union of the chance node i and the distinguishability set $T_{i,j}$ ($T_{i,j} = \{k\}$ in the example from Fig. 3), and the state space is $S_i \cup$ “no observation”. Then, the observation node replaces the node $i \in N^C$ in the information set of $j \in N^D$, controlling whether or not the information in i is available in j . A benefit of this approach is that the modifications are done to the influence diagram, and the RJT formed from the resulting diagram can immediately be used in (2)-(8).

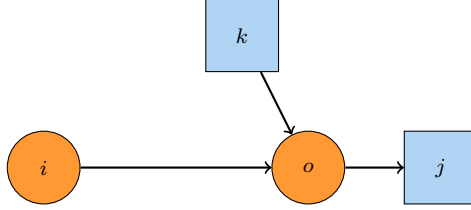


Figure 4: Replacing a distinguishability arc with an observation node in the example from Fig. 3.

One can also utilize the ideas of Ruszczyński (1997) and Apap and Grossmann (2017) for modeling conditional information revelation, in which the information structure can be connected to the decisions by using disjunctive constraints called conditional non-anticipativity constraints (C-NACs). These constraints are similar to the more traditional non-anticipativity constraints (Rockafellar and Wets, 1991) in stochastic programming, but the constraints are only imposed if the distinguishability conditions between pairs of scenarios are not satisfied. These constraints are designed for mixed-integer programming formulations of decision problems and, hence, have not been directly amenable to influence diagram models thus far.

3.2.2. Conditional nonanticipativity constraints (C-NAC)

To integrate C-NACs into our model, we first ease the notation by supplementing the conditional arcs with the *conditional information set* $I_c(j) = \{i \in N^C \cup N^D \mid (i, j) \in A_c\}$ to represent the conditionally available information at node $j \in N^D$. The C-NACs then control whether or not this information is available when making the decision represented by node j . Recall that we require that both the conditional information $I_c(j)$ and the distinguishability set $T_{i,j}$ are a part of the cluster C_j in the rooted junction tree.

C-NACs are used to enforce conditional non-anticipativity when the conditional information states $s_{I_c(j)}$ differ between s_{C_j} and s'_{C_j} . As discussed earlier, if the conditional information states differ (i.e., node $i \in I_c(j)$ has different states in s_{C_j} and s'_{C_j}), distinguishability is dependent on the corresponding condition(s) $F_{i,j}(s_{T_{i,j}})$. This distinguishability of two cluster states at node $j \in N^D$ can be formulated as a Boolean variable $f_j^{s_{C_j}, s'_{C_j}}$, defined as

$$f_j^{s_{C_j}, s'_{C_j}} = \begin{cases} True & \exists i \in I_c(j), s_i \neq s'_i, F_{i,j}(s_{T_{i,j}}) = 1 \\ False & otherwise. \end{cases}$$

The value of $f_j^{s_{C_j}, s'_{C_j}}$ is *True* (i.e., 1) if any node i , for which $s_i \neq s'_i$, is observed when making the decision in j and thus makes scenarios s_{C_j} and s'_{C_j} distinguishable at node j , and *False* (i.e., 0) otherwise.

Finally, we extend the definition of the local decision strategy $Z_j(s_{I(j)})$ and the corresponding binary variables $z(s_j \mid s_{I(j)})$ to include the conditional information set $I_c(j)$. If the value of $f_j^{s_{C_j}, s'_{C_j}}$ is *False*, the local strategies $Z_j(s_{I(j)}, s_{I_c(j)})$ and $Z_j(s_{I(j)}, s'_{I_c(j)})$ must be the same. Note

that we only consider pairs of strategies for which $s_{I(j)}$ is the same, as different non-conditional information states are always distinguishable, precluding the need for C-NACs. Finally, we can define C-NACs in the context of our model as

$$\neg f_j^{s_{C_j}, s'_{C_j}} \implies z(s_j | s_{I(j)}, s_{I_c(j)}) = z(s_j | s_{I(j)}, s'_{I_c(j)}), \forall j \in N^D, s_{C_j}, s'_{C_j} \in S_{C_j}. \quad (10)$$

In light of the above, the C-NACs for binary variables z can also be conveniently written as

$$|z(s_j | s_{I(j)}, s_{I_c(j)}) - z(s_j | s_{I(j)}, s'_{I_c(j)})| \leq f_j^{s_{C_j}, s'_{C_j}}, \forall j \in N^D, s_{C_j}, s'_{C_j} \in S_{C_j}. \quad (11)$$

Notice that the absolute value function used in the left-hand side of (11) can be trivially linearized without significantly increasing the model complexity. This constraint states that for each decision node $j \in N^D$, if the non-conditional information states $s_{I(j)}$ are the same for two cluster states s_{C_j} and s'_{C_j} , and conditionally revealed information does not make these cluster states distinguishable either, the corresponding local decision strategies represented by the z -variables must be the same.

In practice, the main challenge with using C-NACs is that the number of constraints (11) quickly becomes overwhelmingly large. With this in mind, Apap and Grossmann (2017) present several properties that C-NACs possess that can be exploited to reduce the number of such constraints. By making use of these C-NAC reduction properties, representing the decision-dependent information structure within the RJT model is likely to be more compact with C-NACs than the corresponding model using observation nodes, as C-NACs do not require a separate node for modeling the conditional observation.

One limitation of the C-NACs is their implicit assumption that a decision reveals the conditionally observed information with certainty. As such, they cannot be directly employed if the decision reveals the information with a probability of less than one, unlike observation nodes. However, this can easily be circumvented by adding a chance node representing the success/failure of the observation decision and using this new node in the distinguishability function f in (11).

Considering the MIP model (2)-(8), observation nodes result in the conditional probability distribution associated with the observation node setting some probabilities μ to zero. For example, the probability of observing a state other than “no observation” is zero if the distinguishability condition is not fulfilled. On the other hand, C-NACs result in fewer clusters and do not use such extended conditional probability distributions to set μ -variables to zero. Instead, they operate by only imposing equality constraints between decision strategies with indistinguishable information, typically yielding a smaller model. This hypothesis, and the computational performance of the two approaches, are explored in the computational experiments in Section 4.

3.3. Subdiagram decomposition

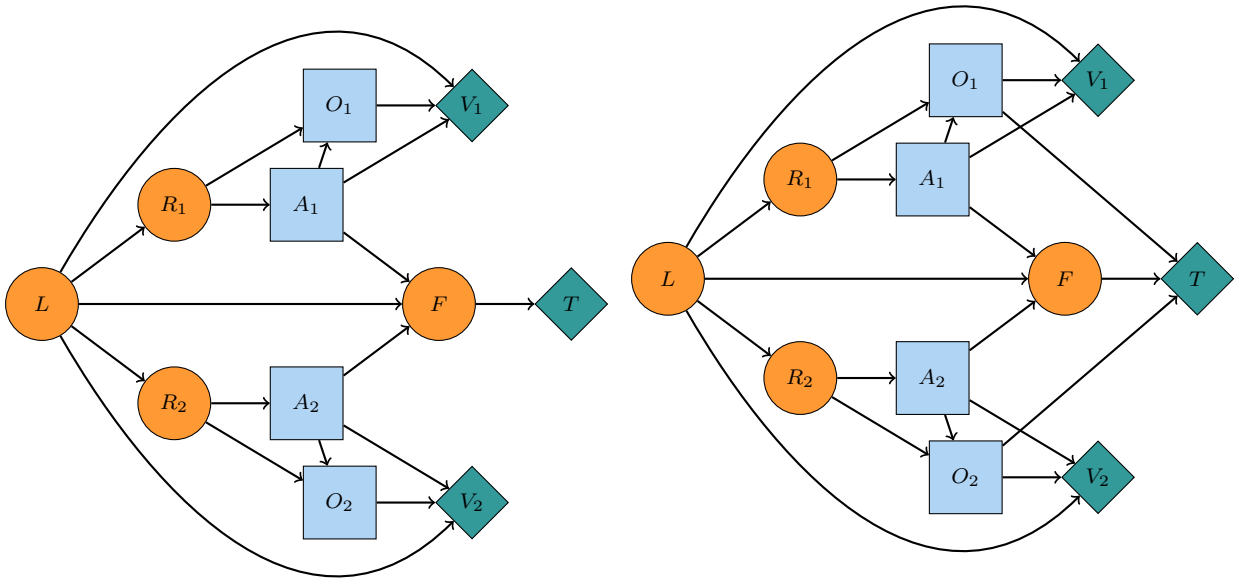
While the MIP formulations in Parmentier et al. (2020) and Salo et al. (2022) offer excellent modeling flexibility for influence diagrams with additional constraints and alternative objective functions, they can only accommodate problems where all decisions have a discrete and finite set of alternatives. However, many problem settings involve decisions that are more naturally modeled as continuous variables. A straightforward approach to make the modeling of these decisions amenable to the proposed MIP formulations is to discretize them with a potentially large number of states. The two main disadvantages of this approach are suboptimal solutions if the discretization fails to accurately represent the decision space, and the increase in model size.

Lee et al. (2021) present a submodel decomposition for influence diagrams based on partitioning the diagram into subdiagrams whose optimal strategies are independent of each other.

However, similarly to Salo et al. (2022) and Parmentier et al. (2020), they only consider influence diagrams with discrete decisions. Our key contribution to exploiting this decomposition is that if we can partition the original diagram into subdiagrams in a way that decision-dependent probabilities and continuous decision variables do not appear in the same subdiagram, we can circumvent the issue of the proposed methods handling Type 3 endogenous uncertainty but not continuous decision variables. Any subdiagram with decision-dependent probabilities and discrete decisions can be solved using the MIP formulation (2)-(8), while alternative methods allowing for continuous decision variables can be used for subdiagrams without decision-dependent probabilities.

While it may seem somewhat restrictive to not allow decision-dependent probabilities and continuous decisions in the same subproblem, this structure is in line with the examples in Hellemo et al. (2018), where first-stage decisions affect the probability distributions in later stages. Additionally, many typical stochastic problems such as facility location (Baron et al., 2008) and unit commitment (Zheng et al., 2014) involve a structure where the discrete decisions in earlier stages affect the continuous decisions in later stages.

We illustrate the decomposition with an extended version of the N-monitoring problem, presented in Fig. 5. To ease the discussion, let us assume the following problem setting: a company is launching a new product, and the product has an initial public interest level represented by node L . There are N sales representatives in different areas, each obtaining a report R_i about the demand level in their location. Based on the report, they decide their production level O_i , with A_i being a discrete decision determining the upper and lower bound for O_i . These discrete decisions are then used to estimate the effect on the overall public interest level F , for which we give a utility value determined by T . In Fig. 5b, the continuous decisions have an effect on the utility T ; in Fig. 5a they do not. This difference will be used to discuss the limitations of the proposed decomposition approach.



(a) N-monitoring problem with continuous decisions

(b) N-monitoring problem with continuous decisions and added influence

Figure 5: Two different influence diagram representations for the N-monitoring problem.

The submodel decomposition can be seen as taking a part of the original diagram and con-

verting it into a value node representing the submodel. However, one cannot simply choose a subset of nodes and make the corresponding part of the diagram a subproblem. Instead, the subproblem must be *stable*, such that the set of relevant hidden variables does not contain any unobserved decision variable (Lee et al., 2021). For a stable submodel, the task of maximizing expected utility within the submodel is independent of the decision strategies outside the submodel.

More formally, a relevant hidden node for decision node d is a node a such that the descendant value nodes N_d^V of d (that is, value nodes to which there is a directed path from d) are not d-separated (Pearl, 2009) from a by either d or $I(d)$. The lack of separation means that a influences the same value node as d , and the influence cannot be determined only knowing the states of $I(d)$ and d . We illustrate this in Fig. 5b with a slightly modified version of the N-monitoring problem that does not lend itself to decomposition. A submodel consisting of nodes O_1 , V_1 and T is not stable in Fig. 5b, because the path $O_2 \rightarrow T$ is not blocked by O_1 or $I(O_1) = \{R_1, A_1\}$ and knowing the decision strategy in O_2 is thus relevant when making the decision in O_1 . For a more thorough treatment of the topic, we refer the reader to Lauritzen and Nilsson (2001) and Lee et al. (2021).

In Fig. 5a, a suitable decomposition is to separate the continuous decision O_i and the associated value node V_i into a subproblem for each $i \in \{1, \dots, N\}$. The utility value of these subproblems depends on L , R_i and A_i , and the decisions A_j and O_j for $j \neq i$ are not relevant in the subproblem i . The subproblems consist of a continuous decision on how much to produce, and the demand represented by L affects the resulting profit, making each subproblem a simple newsvendor problem (Petruzzi and Dada, 1999).

While this decomposition can be a powerful tool for solving influence diagrams, one of the main disadvantages in the context of our MILP models is that, as most solution methods for IDs, it generally only works for “pure” expected utility maximization. For example, if we wanted to impose a chance constraint on the sum of utilities in nodes V_i and T in Fig. 5a, all of the local decision strategies would have to be considered together, making a decomposition approach infeasible.

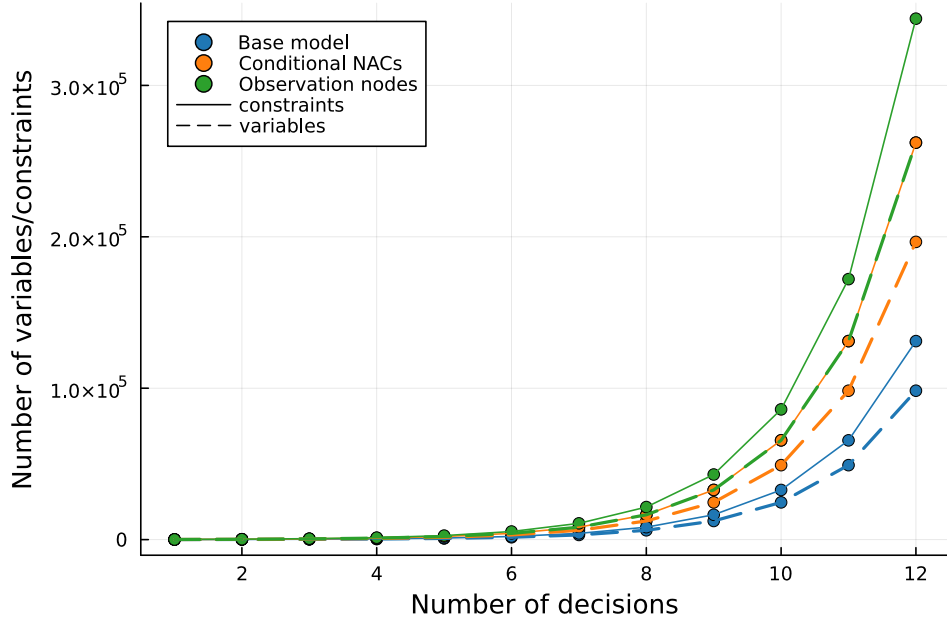
4. Computational experiments

All problems are solved using 8 threads on an Intel E5-2680 CPU at 2.5GHz and 16GB of RAM, provided by the Aalto University School of Science “Science-IT” project. The problem code was implemented in Julia v1.10.3 (Bezanson et al., 2017) with the Gurobi solver v11.0.0 (Gurobi Optimization, LLC, 2022) and JuMP v1.22.1 (Dunning et al., 2017). All the code used in the computational experiments is available at a GitHub repository (Herrala, 2023).

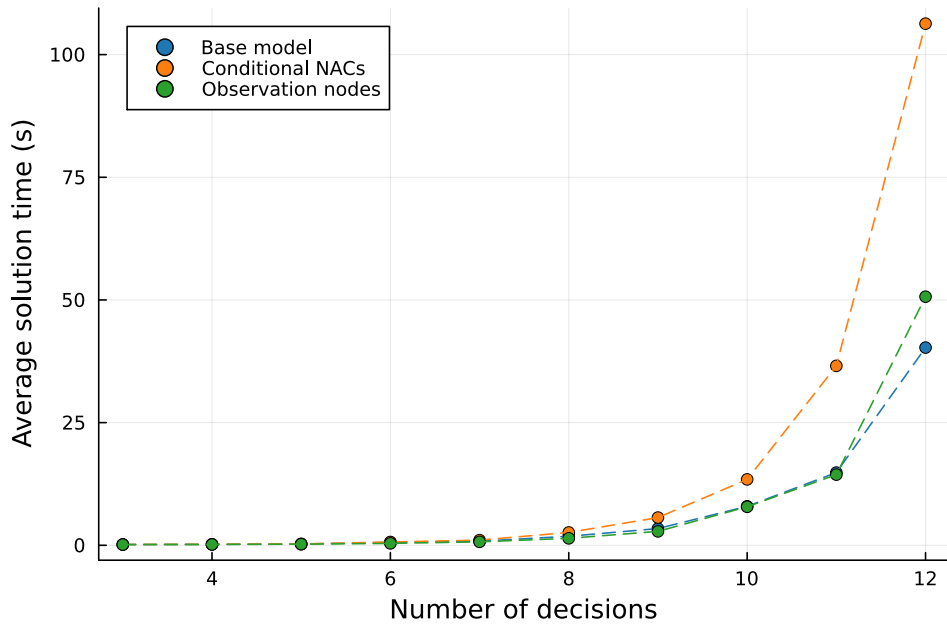
First, we solve the N-monitoring problem with conditionally observed information, varying the number of decision makers. The model sizes and average solution times over 50 randomly parametrized instances are compared between models using observation nodes and C-NACs, and against the original N-monitoring problem (Fig. 1). The results are presented in Fig. 6.

We can see that the number of constraints and variables grows exponentially as more decision makers are considered, approximately doubling as N is increased by one. As expected, the model with C-NACs is significantly smaller than the model using observation nodes when modeling conditionally observed information. However, the solution times for observation nodes are close to those in the model with no conditional information revelation, while the smaller C-NAC model results in significantly longer solution times.

In order to explore the effect of the decomposition and continuous decision variables, we use the version of the N-monitoring problem described in Section 3 with conditionally observed information modeled using C-NACs. We solve 50 instances of the 4-monitoring problem with k randomly selected discrete decision alternatives representing the continuous decision and compare the results to those obtained from the continuous version of the model in Table 1.



(a) Model sizes



(b) Solution times

Figure 6: Model sizes and solution times for the N-monitoring problem with conditionally observed information using C-NACs and observation nodes. “Base model” refers to the model with no conditional observation (Fig. 1).

As discussed earlier in Section 3.3, the subproblems are instances of the newsvendor problem. For such problems, under mild assumptions (positive profit from selling products within the realized demand, negative profit for products exceeding demand), production levels greater than maximum demand or lower than minimum demand are always suboptimal. Thus, we sample the possible decisions (i.e., the states for the decision nodes being discretized) from a uniform distribution between minimum and maximum demand.

It can be seen from the results in Table 1 that a finer discretization results in solutions that are closer to the optimal objective value, but with an increasing computational cost. This rapid increase in solution times requires a tradeoff between computational tractability and solution

# of discrete alternatives k	1	2	3	4	6	8	10	∞
solution time (s)	0.17	0.37	0.89	2.50	6.98	42.24	136.00	0.18
relative objective value	0.911	0.949	0.966	0.964	0.975	0.989	0.997	1

Table 1: Average solution times and objective values for discrete and continuous versions of the problem. Objective values are scaled such that the actual optimal value is 1. The decomposed model with continuous decision is denoted as having infinitely many decision alternatives.

quality. Using the subdiagram decomposition to separate the continuous decision from the diagram results in a solution time similar to the coarsest discretizations and the best possible objective value. This shows that while discretizing continuous variables might be a straightforward solution, it suffers from both high solution times and suboptimal solutions. If the modeler has prior information on the nature of the optimal decisions, the discretization could be more efficient than random sampling from a uniform distribution, but the same issues would persist, albeit lessened.

5. Cost-benefit analysis for climate change mitigation

5.1. Model description

To illustrate the setting, we now consider the cost-benefit analysis on mitigating climate change under uncertainty (see, e.g., Ekholm, 2018). Climate change is driven by greenhouse gas (GHG) emissions and can be mitigated by reducing these emissions, which incurs costs. However, mitigation reduces the negative impacts of climate change, referred to as climate damage. In cost-benefit analysis, the objective is to minimize the discounted sum of mitigation costs and climate damage over a long time horizon. However, multiple uncertainties complicate the analysis.

Here, we consider three salient uncertainties involving both decision-dependent probabilities (Type 1) and conditionally observed information (Type 2). Moreover, some decision nodes involve continuous variables. The resulting problem is a multi-stage mixed-integer nonlinear problem (MINLP) with Type 3 endogenous uncertainty, thus demonstrating the proposed novel features to the rooted junction tree framework described in this paper.

For the mitigation costs, the model considers that technological R&D can be conducted to decrease the costs of bioenergy with carbon capture and storage (BECCS). These R&D decisions can take place at three intensity levels and in two distinct stages. The first stage is a choice between low or medium R&D effort. The low-effort choice represents a business-as-usual perspective, which carries throughout the decision process. If the medium effort is chosen, one observes whether the R&D looks promising or not, and can then decide whether to continue with the medium or switch to a higher R&D effort. The three R&D effort levels and whether the development seems promising or not all affect the probabilities for achieving either low, medium or high mitigation costs later during the century.

The presented model is an extension from Ekholm and Baker (2022), which in turn is a simplification from the SCORE model (Ekholm, 2018). Compared to the formulation proposed here, these earlier analyses have assumed that the uncertainties are resolved exogenously over time and dealt with the mitigation cost uncertainty through separate scenarios. The details of the model structure and parametrization are described in Appendix B.

The influence diagram for the problem is presented in Fig. 7, and a corresponding RJT in Fig. 8. For converting the influence diagram into a rooted junction tree, we use one of the algorithms from Parmentier et al. (2020). The algorithm takes a set of nodes and their information sets, along with a topological order for the nodes and returns a gradual rooted junction tree. A topological order for a graph assigns a unique index to each node, so that for each arc $(i, j) \in A_{ID}$, the index of node j is larger than that of node i .

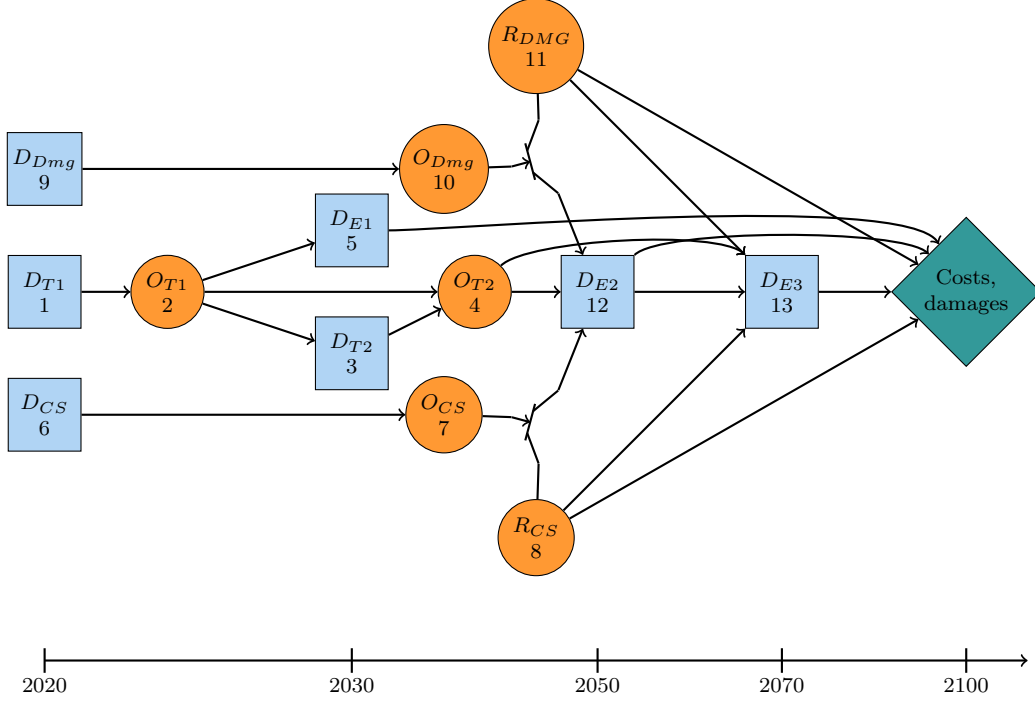


Figure 7: Influence diagram of the climate change cost-benefit problem with endogenous uncertainty due to R&D. We assume that all prior decisions and uncertainty realizations apart from the conditionally observed parameters are remembered when making decisions, but omit the arcs for clarity. Additionally, the individual value nodes associated with decision nodes 1, 3, 6 and 9 are omitted for clarity. The nodes are numbered according to the topological order used for forming the RJT.

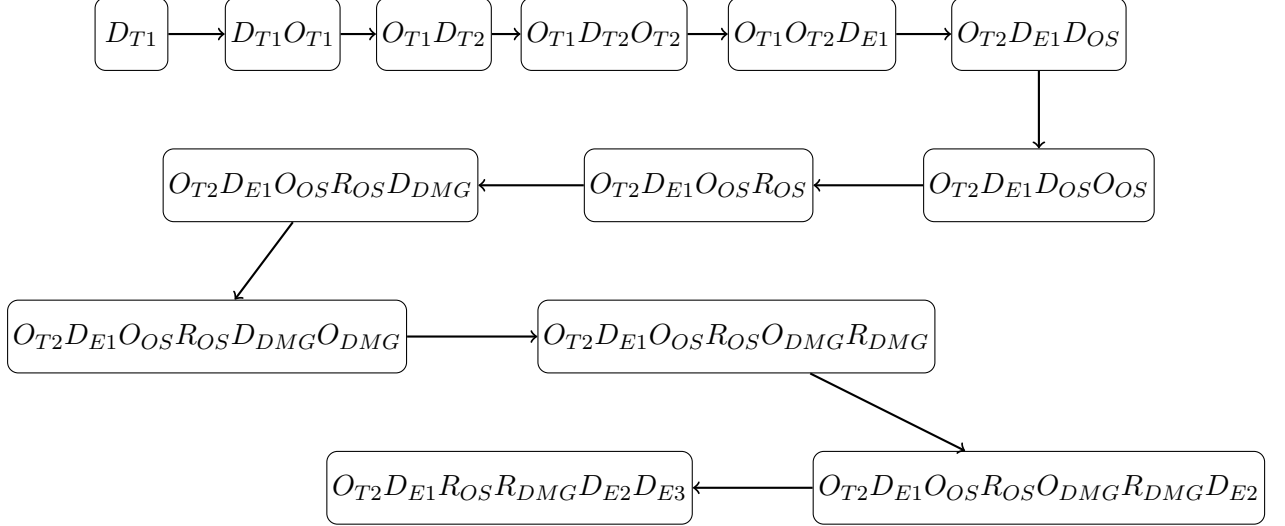


Figure 8: A rooted junction tree representation of the ID in Fig. 7

The first stage of the diagram involves R&D decisions towards climate sensitivity (D_{CS}), damages (D_{Dmg}) and technology (D_{T1}). If successful, the climate parameter (climate sensitivity and damage exponent) R&D efforts modify the information structure so that the parametrization is partially revealed in 2050 instead of 2070. This is represented by the nodes R_{Dmg} and R_{CS} and the outcome (success/failure) of the projects by O_{Dmg} and O_{CS} . Because the value nodes $v \in N^V$ represent deterministic mappings $s_{I(v)} \rightarrow \mathbb{R}$, the value nodes are not explicitly represented in the RJT. Instead, the components of the expected utility can be extracted

from the clusters containing $I(v)$, following the ideas used in the computational experiments of Parmentier et al. (2020).

Decisions over emission reductions ($D_{Ei}, i \in \{1, 2, 3\}$) are made in three stages: in 2030, 2050 and 2070, which represent the medium-term and long-term climate actions. The technological R&D potentially lowers the costs of emission reductions in 2050 and 2070. We connect our example to the discussion on the feasibility of large-scale deployment of BECCS, which has been a crucial but contested result of many mitigation scenarios (Calvin et al., 2021). The R&D costs and probabilities for the three levels of BECCS costs are parametrized using expert-elicited estimates in Baker et al. (2015). These are then reflected in the overall emission reduction costs. It is worth noting the major challenges in long-term technological foresight, which is manifested in the wide spectrum of responses from the experts; but elicitation data is nevertheless useful for illustrating the importance of technological progress. After 2070, the level of climate change is observed based on the chosen emission reductions and the observed branch of climate sensitivity, which then determines the severity of the climate damages along with the observed branch of climate damages.

5.2. Modifying the influence diagram

As discussed in Section 3, the original formulation is limited to problems with discrete and finite state spaces for all nodes. However, discretizing the emission levels $D_{Ei}, i \in \{1, 2, 3\}$ would inevitably result in suboptimal solutions, thereby limiting the representability of the naturally continuous nature of the decision variables representing the emission levels.

Following the ideas in Section 3.3, we modify the influence diagram and move the nodes $D_{Ei}, i \in \{1, 2, 3\}$ to a subproblem whose solution becomes the utility value in the main problem. Additionally, we place all chance nodes except O_{T1} in the subproblem, resulting in the decomposition presented in Fig. 9. It should be noted that the choice of which nodes to include in the subproblem is not unique, and for larger models, a significant tradeoff between submodel and main problem sizes might be present, affecting the total solution time. Nevertheless, for this illustrative example, the solution times are small (they are discussed in Section 5.4) making the analysis of secondary importance in our context.

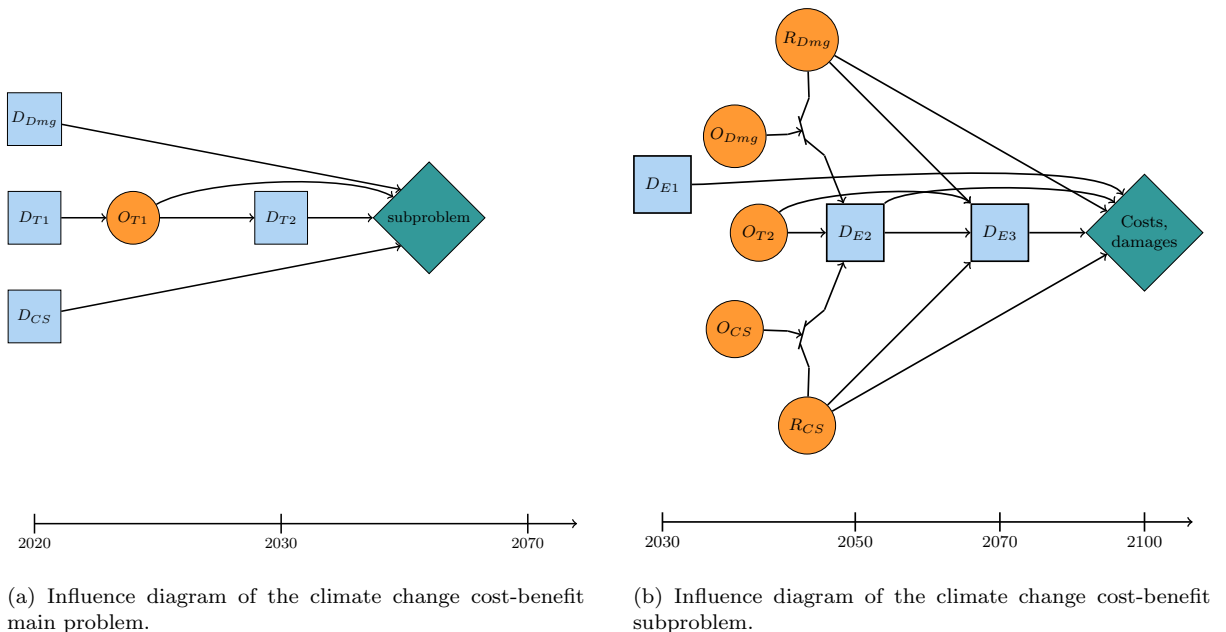


Figure 9: The decomposed climate change cost-benefit problem.

In the resulting subproblem in Fig. 9b, there is no Type 1 endogenous uncertainty. Hence, the subproblem can be modeled as a nonlinear three-stage stochastic programming problem

with continuous decision variables. The nonlinearity stems from the SCORE model described in Appendix B.

5.3. Model results

The optimal R&D strategy for this problem is to carry out all R&D projects. Fig. 10 presents the emission levels of the optimal mitigation strategy. The effect of the technology R&D on optimal emission pathways is shown with the three subfigures corresponding to the final R&D outcome after 2030. Intuitively, successful research and therefore cheaper abatement leads to more abatement. This has also a major impact on the total costs of the optimal strategy: with the low cost curves, the total expected cost is roughly 30% lower than with medium costs, and with high abatement costs 30% higher than with the medium cost curve.

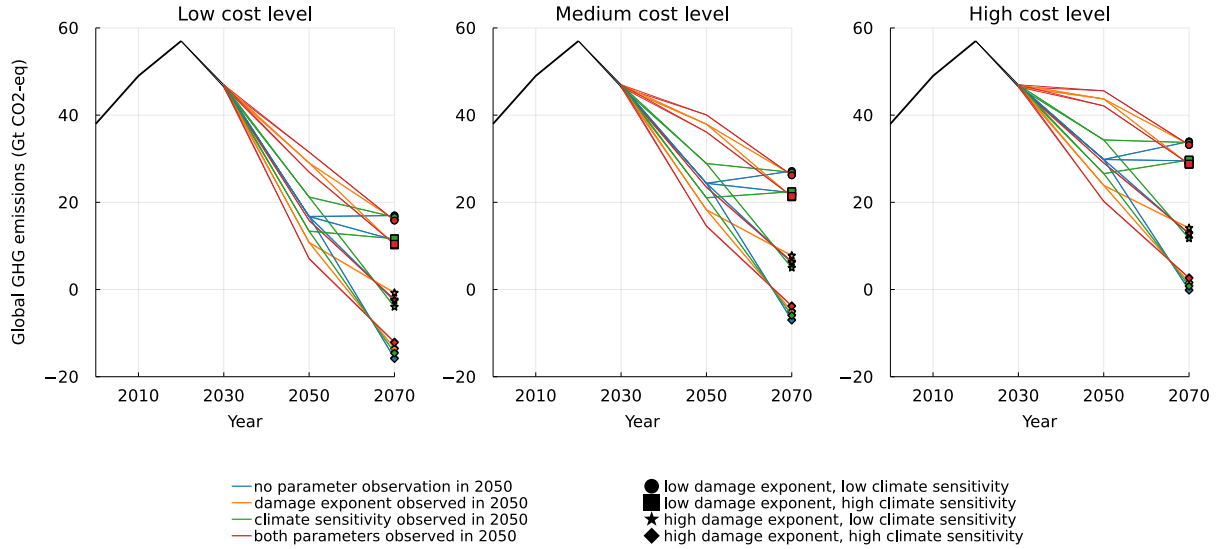


Figure 10: Abatement levels for different outcomes of technology research and parameter observations in 2030.

The climatic parameter R&D, the other endogenous effect in this model has a magnitude smaller effect on the expected costs than the technology R&D, but the effect on abatement levels is remarkable. The branches after 2030 represent different realizations of the technology research and partial learning of the climate parameters. If the research efforts for both parameters fail (blue lines in Fig. 10), the 2050 abatement decisions are made knowing only the outcome of the technology projects, and the four scenarios of partial learning only occur after 2050. Learning the parameters before 2050 results in more dispersed abatement strategies. Finally, the underlying parameter branching is represented with shapes in 2070. It can be seen that the impact of climate sensitivity is considerably smaller than that of the damage exponent. This is in line with the results in Ekholm and Baker (2022) and shows that the proposed framework could be applied in planning for optimal R&D pathways.

5.4. Computational aspects

Using the decomposed model presented in Fig. 9, the main problem is solved in 0.4 seconds, while solving all of the subproblems takes one second. If we instead solve a problem corresponding to Fig. 7 without decomposition, the framework requires discretizing the abatement levels. Using discrete decision spaces to approximate a continuous variable leads to suboptimal solutions. Furthermore, even with only five levels for each abatement decision, the problem becomes more computationally demanding than the continuous version. The damage costs are calculated in a tenth of a second, but solving the model takes four seconds. As suggested by the experiments in Section 4, in larger problems, the discretized problem could quickly become intractable. The decomposed problem instead uses continuous decision variables to represent

the abatement decisions, precluding the need for a discretization. As a consequence, it is faster to solve than the rudimentary approximation with five abatement levels.

The discretized model has 2172 constraints and 4332 variables, of which 327 are binary; and the main problem of the decomposed model has 40 constraints and 66 variables, of which 12 are binary. The discretized model is thus two orders of magnitude larger than the decomposed model, but the damage costs in the discretized model are calculated almost instantaneously. However, the trade-off of moving some of the computational burden into the subproblems makes it possible to solve the continuous problem to optimality. Overall, this case study provides an illustrative example of an application where the developments in this paper make it possible to consider settings that are challenging both from modeling and computational standpoints.

6. Conclusion

In this paper, we propose a framework for Type 3 endogenously uncertain stochastic programming (T3ESP) problems. Our contributions consist of comparing two different modeling approaches to consider conditionally observed information, making the framework more generally applicable to decision-making problems. The proposed framework is based on the work by Parmentier et al. (2020), originally developed for solving decision problems with decision-dependent uncertainties by converting an influence diagram representation of the problem to a mixed-integer programming (MIP) model.

To the best of our knowledge, and in line with Hellemo et al. (2018), Type 3 endogenously uncertain stochastic programming (T3ESP) problems have not been previously addressed in the literature. To make the rooted junction tree (RJT) formulations applicable to such problems, we show how Type 2 endogenous uncertainties can be modeled by either modifying the underlying influence diagram by adding observation nodes or by incorporating conditional non-anticipativity constraints (C-NACs) to the MIP model. We note that with minimal modifications, the developments presented in this paper can also be applied to extend the Decision Programming framework (Salo et al., 2022; Hankimaa et al., 2023), as the structure of the two MIP models is sufficiently similar.

In practice, both approaches have their advantages and disadvantages. Adding observation nodes only requires modifying the influence diagram by adding new nodes, while C-NACs are additional constraints that must be added to the MIP model. From the standpoint of a practitioner, it would be simpler to not require explicit modification of the resulting model. On the other hand, if one allows for modifying the MIP model by using C-NACs, this might also allow for representing other parts of the decision process explicitly as added variables or constraints. Further research in this direction is thus relevant.

However, if decision-dependent probability distributions and conditional information revelation are intertwined in the problem structure, for example, by the presence of imperfect conditional observations, one cannot directly employ C-NAC constraints. An example of such a problem would be a version of the climate CBA problem in Section 5 where the climate parameter research does not reveal the correct branch, that is, remove one of the extreme parameter values, but instead gives a probability distribution that provides better information than the original. Observation nodes can be used for modeling such uncertainties, while C-NACs require additional modifications to the diagram, further diminishing their benefits. Finally, the MIP models with C-NACs are smaller than the corresponding models using observation nodes, which is in general a desirable feature. In our experiments, however, having smaller MIP models did not translate into improved computational efficiency. Nevertheless, further research is required before more can be concluded in that direction.

Considering alternative modeling paradigms would make the framework suitable for a broader set of problems. Interesting examples of such research ideas are (distributionally) robust optimization and further examination of multi-objective decision-making. For large problems, it

might be necessary to improve the computational performance using, e.g., decomposition methods for solving the MIP model (2)-(8), and solution heuristics. In this paper, we explore the use of influence diagram decomposition (e.g., Lee et al., 2021) for improving the computational efficiency of finding maximum expected utility strategies for influence diagrams. Perhaps more interestingly, in the context of our MIP formulations, we also show that such decomposition approaches can allow for solving decision problems with continuous decision variables, significantly improving the general applicability of the formulation.

In conclusion, the proposed developments turned the framework sufficiently general to model a challenging example problem with Type 3 endogenous uncertainty. It should also be noted that the influence diagrams are formulated as MILP problems, guaranteeing global optimality of solutions despite the challenging nature of the underlying decision problems.

Acknowledgements

Funding: The work of Herrala and Oliveira was supported by the Research Council of Finland [*Decision Programming: A Stochastic Optimization Framework for Multi-Stage Decision Problems*, grant number 332180]; the work of Ekholm was supported by the Research Council of Finland [*Designing robust climate strategies with Negative Emission Technologies under deep uncertainties and risk accumulation (NETS)*, grant number 331764].

Appendix A. Notation

symbol	description
$G_{ID} = (N, A_{ID})$	an influence diagram consisting of nodes $n \in N$ and arcs $a \in A_{ID}$
N^C, N^D, N^V	sets of chance, decision and value nodes, respectively
$I(j)$	information set of node $j \in N$: $I(j) = \{i \in N \mid (i, j) \in A_{ID}\}$
$s_j \in S_j$	state of node j
$s_X \in S_X$	states of nodes in set X : $s_X = (s_j)_{j \in X}$
$G_{RJT} = (V, A_{RJT})$	a rooted junction tree consisting of clusters $C \in V$ and arcs $(C_i, C_j) \in A_{RJT}$
Z_j	local decision strategy in node $j \in N^D$ mapping $s_{I(j)}$ to a decision s_j
$z(s_j \mid s_{I(j)})$	a binary decision variable with value 1 if and only if Z_j maps $s_{I(j)}$ to s_j
$\mathbb{P}(X_j = s_j \mid X_{I(j)} = s_{I(j)})$	conditional probability of node $j \in N^C$ being in state s_j given $s_{I(j)}$
μ_{C_j}	the joint probability distribution of nodes $n \in C_j$
u_{C_j}	utility function mapping s_{C_j} to a real-valued utility value

Table A.2: Notation used for influence diagrams and rooted junction trees

symbol	description
$T_{i,j}$	distinguishability set, the nodes that are involved in making node $i \in N^C \cup N^D$ observed in node $j \in N^D$
$F_{i,j}$	distinguishability condition for observing node $i \in N^C \cup N^D$ in node $j \in N^D$
$a_c \in A_c$	conditional arcs
$I_c(j)$	conditional information set of node j
$f_j^{s_{C_j}, s'_{C_j}}$	a Boolean variable with value 1/True if and only if s_{C_j} and s'_{C_j} are distinguishable when making decision j

Table A.3: Notation used for conditionally observed information

Appendix B. Cost-benefit model description

The idea in climate change cost-benefit analysis (CBA) is the minimization of emission reduction costs and climate damages. The abatement cost calculation is based on marginal abatement cost curves, as presented in equation (B.1), using numerical estimates from the SCORE model (Ekholm, 2018). Coefficients α and β are the parameters of the cost curves, R is the total abatement level and c is the marginal cost of abatement. In (B.3), C is the total cost for abatement level R . The subscript t has been omitted for clarity, but parameters α and β change between stages due to assumed technological progress.

$$R = \alpha c^\beta \tag{B.1}$$

$$\implies c = \left(\frac{R}{\alpha}\right)^{1/\beta} \tag{B.2}$$

$$\implies C = \int_0^R \left(\frac{r}{\alpha}\right)^{1/\beta} dr = \frac{\beta}{1+\beta} \left(\frac{1}{\alpha}\right)^{1/\beta} R^{1+1/\beta}. \tag{B.3}$$

The uncertainties considered in this analysis concern 1) the sensitivity of climate to GHG emissions, 2) the severity of climate change damages to society, and 3) the cost of reducing emissions. Decisions can be made to first conduct costly research and development (R&D) efforts towards each source of uncertainty. For the uncertainties regarding climate sensitivity and damages, a successful R&D effort results in an earlier revelation of the parametrization, whereas an unsuccessful or no R&D effort reveals this information later. Similar models of R&D pipeline optimization under (Type 2) endogenous uncertainty are considered in Colvin and Maravelias (2011).

Departing from the predetermined technological progress that was assumed by Ekholm (2018), the parameter α in the model depends here on the result of technological R&D, as presented in Figure 7. We consider three levels of R&D effort in 2020 and 2030, which can then lead to three possible levels of MAC curves for years 2050 and 2070. For a related discussion, we refer the reader to Rathi and Zhang (2022), who consider endogenous technology learning on power generation.

For the effect of R&D efforts on bioenergy and carbon capture and storage (CCS) costs, we used expert elicited estimates from Baker et al. (2015). To convert these into emission reduction costs, we assume a coal power plant as a baseline and calculate the additional costs from bioenergy with carbon capture and storage (BECCS) relative to the amount of reduced emissions by switching from coal to BECCS. Both plants were assumed to have a lifetime of 30 years and operate at 80% capacity on average. The coal power plant was assumed to have a 40% efficiency and produce 885 tonnes of CO₂ per GWh of electricity. The generation cost was assumed to be 50\$/MWh. Costs were discounted at 5% rate.

Compared to coal, BECCS accrues additional costs per generated unit of electricity from the higher cost of biofuel and lower efficiency, and the additional investment to CCS and loss of efficiency from using some of the generated electricity in the carbon capture process. Baker et al. (2015) presented probability distributions for these parameters following three different levels of R&D efforts (low, medium and high). To calculate the cost differential to coal power plant, we performed a Monte Carlo sampling of these four parameters, separately for each R&D level, which was then compared to the amount of reduced emissions per generated unit of electricity. This yields a distribution of emission reduction costs for BECCS for each R&D level.

We generalize the impact of R&D on BECCS's emission reduction cost to the overall marginal abatement cost (MAC) curve. This is obviously a simplification, but nevertheless reflects the major role that BECCS might have in decarbonizing the economy (e.g. Fuss et al., 2018; Rogelj et al., 2018). We take the high MAC from Ekholm (2018) as the starting point and define two MAC curves that are proportionally scaled down from the high MAC.

The low R&D level yields an average emission reduction cost of around 100 \$/t. We set three bins for three cost levels: high costs correspond to above 75 \$/t, medium costs are between 25 and 75 \$/t, and low costs are below 25 \$/t. The probabilities of achieving high, medium or low emission reduction costs are then estimated from the Monte Carlo sampling for each R&D level, and presented in Table B.4. With medium and high R&D effort, the average cost in the low cost bin is around 20 \$/t. Therefore we assign the reduction in the MAC as 50% for medium costs and 80% for low costs. The corresponding parameters are listed in Table B.5. These are still within the range of costs used in Ekholm (2018), where the low-cost MAC yielded the same emission reductions than the high-cost MAC with approximately 90% lower costs in 2050.

Table B.4: Probabilities for different abatement costs (rows) with different levels of R&D effort (columns).

	Low R&D	Medium R&D	High R&D
High costs	73 %	31 %	9 %
Medium costs	27 %	64 %	73 %
Low costs	0 %	5 %	18 %

Table B.5: Cost curve parametrization

year	α_{high}	α_{medium}	α_{low}	β
2030	3.57	3.57	3.57	0.340
2050	11.2	13.3	16.7	0.250
2070	21.1	24.3	29.3	0.203

The climate damage cost calculation is from DICE (Nordhaus, 2017). The damage function is presented in (B.4), where $Y(t)$ is the world gross economic output at time t , a is a scaling parameter and b is the damage exponent. While climate change and the abatement decisions have an effect on the economic output, the effect is assumed small and $Y(t)$ is defined exogenously in SCORE.

$$D(t, \Delta T) = Y(t)a\Delta T^b. \quad (\text{B.4})$$

Finally, the temperature change ΔT is approximated with (B.5), where c is the climate sensitivity (the temperature increase from doubling of CO₂ emissions), M is the sum of emissions in 2030-2070 and k_i are coefficients.

$$\Delta T = k_1cM + k_2c + k_3M + k_4. \quad (\text{B.5})$$

In SCORE, both the DICE damage parameter and the climate sensitivity are uncertain with three options, low, medium and high, as presented in Table B.6, and the uncertainty is revealed in two steps in a binomial lattice. First, between 2050 and 2070, one of the extreme alternatives is removed from both uncertainties, that is, for both parameters, we know either that the value is not high or that it is not low. Then, after 2070, we learn the actual value.

The implementation here combines influence diagrams and MSSP in a way that the underlying branching probabilities are used as the probabilities of the observations R_{Dmg} and R_{CS} in Fig. 7. For the damage exponent, all branching probabilities are 50%. The observation R_{Dmg} thus has a 50% probability of removing either the high or low value. Depending on the branch, the low or high value then has a 50% probability in the later branching, with the other 50% for the medium value. This makes the medium branch have a 50% probability in total, while the two extreme values both have a 25% probability. For the climate sensitivity, the first branching is with a 50% probability for both branches. However, the second branching is different. If the high sensitivity is excluded in the first branch, there is a 21% conditional probability of the low branch in the second branching, meaning a 10.5% total probability for the low sensitivity.

Similarly, there is a 23% conditional probability of high damages in the other branch, resulting in a 11.5% probability for the high sensitivity. The remaining 78% is the final probability of medium sensitivity.

Table B.6: Climate sensitivity and damage exponent values

	Climate sensitivity	Damage exponent
High	6	4
Medium	3	2
Low	1.5	1

This uncertain process is modeled by means of a multi-stage stochastic programming problem, where new information is obtained gradually. It is possible to perform research on these parameters. If the research succeeds, one of the extreme values is excluded already before 2050, revealing the first branching in the observation process earlier than without or with failed research. The observation of the actual parameter value (the second branching) still happens after 2070, after all abatement decisions have been made. The total cost we aim to minimize is then a discounted sum of research costs, abatement costs (B.3) for years 2030, 2050 and 2070, and damage costs (B.4).

Appendix C. MIP formulation of the 2-monitoring problem

$$\begin{aligned} \max \quad & \sum_{s_{A_1} \in S_{A_1}, s_{V_1} \in S_{V_1}} \mu_{C_{V_1}}(s_{A_1}, s_{V_1}) u_{V_1}(s_{A_1}, s_{V_1}) + \sum_{s_{A_2} \in S_{A_2}, s_{V_2} \in S_{V_2}} \mu_{C_{V_2}}(s_{A_2}, s_{V_2}) u_{V_2}(s_{A_2}, s_{V_2}) \\ & + \sum_{s_F \in S_F, s_T \in S_T} \mu_{C_T}(s_F, s_T) u_T(s_F, s_T) \end{aligned} \quad (\text{C.1})$$

$$\text{s.t.} \quad \sum_{s_L \in S_L} \mu_{C_L}(s_L) = 1, \quad (\text{C.2})$$

$$\mu_{C_L}(s_L) = \mathbb{P}(X_L = s_L), \quad \forall s_L \in S_L \quad (\text{C.3})$$

$$\mu_{C_L}(s_L) \geq 0, \quad \forall s_L \in S_L \quad (\text{C.4})$$

$$\sum_{s_L \in S_L, s_{R_1} \in S_{R_1}} \mu_{C_{R_1}}(s_L, s_{R_1}) = 1, \quad (\text{C.5})$$

$$\mu_{C_L}(s_L^*) = \sum_{s_{R_1} \in S_{R_1}} \mu_{C_{R_1}}(s_L^*, s_{R_1}), \quad \forall s_L^* \in S_L \quad (\text{C.6})$$

$$\mu_{C_{R_1}}(s_L, s_{R_1}) = \mu_{\bar{C}_{R_1}}(s_L) \mathbb{P}(X_{R_1} = s_{R_1} \mid X_L = s_L), \quad \forall s_L \in S_L, s_{R_1} \in S_{R_1} \quad (\text{C.7})$$

$$\mu_{C_{R_1}}(s_L, s_{R_1}) \geq 0, \quad \forall s_L \in S_L, s_{R_1} \in S_{R_1} \quad (\text{C.8})$$

$$\sum_{s_L \in S_L, s_{R_1} \in S_{R_1}, s_{A_1} \in S_{A_1}} \mu_{C_{A_1}}(s_L, s_{R_1}, s_{A_1}) = 1, \quad (\text{C.9})$$

$$\mu_{C_{R_1}}(s_L^*, s_{R_1}^*) = \sum_{s_{A_1} \in S_{A_1}} \mu_{C_{A_1}}(s_L^*, s_{R_1}^*, s_{A_1}), \quad \forall s_L^* \in S_L, s_{R_1}^* \in S_{R_1}^* \quad (\text{C.10})$$

$$\mu_{C_{A_1}}(s_L, s_{R_1}, s_{A_1}) = \mu_{\bar{C}_{A_1}}(s_L, s_{R_1}) z(s_{A_1} \mid s_{R_1}), \quad \forall s_L \in S_L, s_{R_1} \in S_{R_1}, s_{A_1} \in S_{A_1} \quad (\text{C.11})$$

$$\mu_{C_{A_1}}(s_L, s_{R_1}, s_{A_1}) \geq 0, \quad \forall s_L \in S_L, s_{R_1} \in S_{R_1}, s_{A_1} \in S_{A_1} \quad (\text{C.12})$$

$$z(s_{A_1} \mid s_{R_1}) \in \{0, 1\}, \quad \forall s_{R_1} \in S_{R_1}, s_{A_1} \in S_{A_1} \quad (\text{C.13})$$

$$\sum_{s_{A_1} \in S_{A_1}, s_{V_1} \in S_{V_1}} \mu_{C_{V_1}}(s_{A_1}, s_{V_1}) = 1, \quad (\text{C.14})$$

$$\sum_{s_L \in S_L, s_{R_1} \in S_{R_1}} \mu_{C_{A_1}}(s_L, s_{R_1}, s_{A_1}^*) = \sum_{s_{V_1} \in S_{V_1}} \mu_{C_{V_1}}(s_{A_1}^*, s_{V_1}), \quad \forall s_{A_1}^* \in S_{A_1} \quad (\text{C.15})$$

$$\mu_{C_{V_1}}(s_{A_1}, s_{V_1}) = \mu_{\bar{C}_{V_1}}(s_{A_1}) \mathbb{P}(X_{V_1} = s_{V_1} \mid X_{A_1} = s_{A_1}), \quad \forall s_{A_1} \in S_{A_1}, s_{V_1} \in S_{V_1} \quad (\text{C.16})$$

$$\mu_{C_{V_1}}(s_{A_1}, s_{V_1}) \geq 0, \quad \forall s_{A_1} \in S_{A_1}, s_{V_1} \in S_{V_1} \quad (\text{C.17})$$

...

References

- Apap, R.M., Grossmann, I.E., 2017. Models and computational strategies for multistage stochastic programming under endogenous and exogenous uncertainties. *Computers & Chemical Engineering* 103, 233–274. <https://doi.org/10.1016/j.compchemeng.2016.11.011>.
- Baker, E., Bosetti, V., Anadon, L.D., Henrion, M., Aleluia Reis, L., 2015. Future costs of key low-carbon energy technologies: Harmonization and aggregation of energy technology expert elicitation data. *Energy Policy* 80, 219–232. <https://doi.org/10.1016/j.enpol.2014.10.008>.
- Baron, O., Berman, O., Krass, D., 2008. Facility location with stochastic demand and constraints on waiting time. *Manufacturing & Service Operations Management* 10, 484–505.

- Bezanson, J., Edelman, A., Karpinski, S., Shah, V.B., 2017. Julia: A fresh approach to numerical computing. *SIAM Review* 59, 65–98. <https://doi.org/10.1137/141000671>.
- Bielza, C., Gómez, M., Shenoy, P.P., 2011. A review of representation issues and modeling challenges with influence diagrams. *Omega* 39, 227–241.
- Boland, N., Dumitrescu, I., Froyland, G., 2008. A multistage stochastic programming approach to open pit mine production scheduling with uncertain geology. *Optimization online* , 1–33.
- Calvin, K., Cowie, A., Berndes, G., Arneth, A., Cherubini, F., Portugal-Pereira, J., Grassi, G., House, J., Johnson, F.X., Popp, A., Rounsevell, M., Slade, R., Smith, P., 2021. Bioenergy for climate change mitigation: scale and sustainability. *GCB Bioenergy* 13, 1346–1371. <https://doi.org/10.1111/gcbb.12863>.
- Colvin, M., Maravelias, C.T., 2010. Modeling methods and a branch and cut algorithm for pharmaceutical clinical trial planning using stochastic programming. *European Journal of Operational Research* 203, 205–215. <https://doi.org/10.1016/j.ejor.2009.07.022>.
- Colvin, M., Maravelias, C.T., 2011. R&d pipeline management: Task interdependencies and risk management. *European Journal of Operational Research* 215, 616–628. <https://doi.org/10.1016/j.ejor.2011.06.023>.
- Detwarasiti, A., Shachter, R.D., 2005. Influence diagrams for team decision analysis. *Decision Analysis* 2, 207–228.
- Dunning, I., Huchette, J., Lubin, M., 2017. JuMP: A Modeling Language for Mathematical Optimization. *SIAM Review* 59, 295–320. <https://doi.org/10.1137/15M1020575>.
- Dupačová, J., 2006. Optimization under exogenous and endogenous uncertainty, in: *Proceedings of the 24th International conference on Mathematical Methods in Economics*, pp. 131–136. <https://doi.org/10.13140/2.1.2682.2089>.
- Ekholm, T., 2018. Climatic Cost-benefit Analysis Under Uncertainty and Learning on Climate Sensitivity and Damages. *Ecological Economics* 154, 99–106. <https://doi.org/10.1016/j.ecolecon.2018.07.024>.
- Ekholm, T., Baker, E., 2022. Multiple Beliefs, Dominance and Dynamic Consistency. *Management Science* 68, 529–540. <https://doi.org/10.1287/mnsc.2020.3908>.
- Escudero, L.F., Garín, M.A., Monge, J.F., Unzueta, A., 2020. Some matheuristic algorithms for multistage stochastic optimization models with endogenous uncertainty and risk management. *European Journal of Operational Research* 285, 988–1001. <https://doi.org/10.1016/j.ejor.2020.02.046>.
- Fuss, S., Lamb, W.F., Callaghan, M.W., Hilaire, J., Creutzig, F., Amann, T., Beringer, T., De Oliveira Garcia, W., Hartmann, J., Khanna, T., Luderer, G., Nemet, G.F., Rogelj, J., Smith, P., Vicente, J.V., Wilcox, J., Del Mar Zamora Dominguez, M., Minx, J.C., 2018. Negative emissions - Part 2: Costs, potentials and side effects. *Environmental Research Letters* 13. <https://doi.org/10.1088/1748-9326/aabf9f>.
- Goel, V., Grossmann, I.E., 2006. A Class of stochastic programs with decision dependent uncertainty. *Mathematical Programming* 108, 355–394. <https://doi.org/10.1007/s10107-006-0715-7>.
- Gurobi Optimization, LLC, 2022. Gurobi Optimizer Reference Manual. URL: <https://www.gurobi.com>.

- Hankimaa, H., Herrala, O., Oliveira, F., Tollander de Balsch, J., 2023. Decisionprogramming.jl – a framework for modelling decision problems using mathematical programming. [arXiv:2307.13299](https://arxiv.org/abs/2307.13299).
- Hellemo, L., Barton, P.I., Tomasgard, A., 2018. Decision-dependent probabilities in stochastic programs with recourse. *Computational Management Science* 15, 369–395. <https://doi.org/10.1007/s10287-018-0330-0>.
- Herrala, O., 2023. Source code repository: Type 2 RJT. URL: <https://github.com/solliolli/type2-rjt>.
- Herrala, O., Terho, T., Oliveira, F., 2023. Risk measures in rooted junction tree models. In preparation .
- Howard, R.A., Matheson, J.E., 2005. Influence diagrams. *Decision Analysis* 2, 127–143. <https://doi.org/10.1287/deca.1050.0020>.
- Jonsbråten, T.W., Wets, R.J., Woodruff, D.L., 1998. A class of stochastic programs with decision dependent random elements. *Annals of Operations Research* 82, 83–106. <https://doi.org/10.1023/A:1018943626786>.
- Lauritzen, S.L., Nilsson, D., 2001. Representing and solving decision problems with limited information. *Management Science* 47, 1235–1251. <https://doi.org/10.1287/mnsc.47.9.1235.9779>.
- Lee, J., Marinescu, R., Dechter, R., 2021. Submodel decomposition bounds for influence diagrams, in: *Proceedings of the AAAI Conference on Artificial Intelligence*, pp. 12147–12157.
- Li, X., Liu, Q., 2023. Strategic ignorance: Managing endogenous demand in a supply chain. *Omega* 114, 102729. <https://doi.org/10.1016/j.omega.2022.102729>.
- Mitra, G., Lucas, C., Moody, S., Hadjiconstantinou, E., 1994. Tools for reformulating logical forms into zero-one mixed integer programs. *European Journal of Operational Research* 72, 262–276.
- Nordhaus, W.D., 2017. Revisiting the social cost of carbon. *Proceedings of the National Academy of Sciences* 114, 1518–1523. <https://doi.org/10.1073/pnas.1609244114>.
- Parmentier, A., Cohen, V., Leclère, V., Obozinski, G., Salmon, J., 2020. Integer programming on the junction tree polytope for influence diagrams. *INFORMS Journal on Optimization* 2, 209–228.
- Pearl, J., 2009. *Causality*. Cambridge university press.
- Peeta, S., Sibel Salman, F., Gunnec, D., Viswanath, K., 2010. Pre-disaster investment decisions for strengthening a highway network. *Computers and Operations Research* 37, 1708–1719. <https://doi.org/10.1016/j.cor.2009.12.006>.
- Petruzzi, N.C., Dada, M., 1999. Pricing and the newsvendor problem: A review with extensions. *Operations research* 47, 183–194.
- Piccione, M., Rubinstein, A., 1997. On the interpretation of decision problems with imperfect recall. *Games and Economic Behavior* 20, 3–24.
- Raiffa, H., 1968. *Decision analysis : introductory lectures on choices under uncertainty*. Random House, New York.

- Rathi, T., Zhang, Q., 2022. Capacity planning with uncertain endogenous technology learning. *Computers & Chemical Engineering* 164, 107868. <https://doi.org/10.1016/j.compchemeng.2022.107868>.
- Rockafellar, R.T., Wets, R.J.B., 1991. Scenarios and policy aggregation in optimization under uncertainty. *Mathematics of operations research* 16, 119–147. <https://doi.org/10.1287/moor.16.1.119>.
- Rogelj, J., Popp, A., Calvin, K.V., Luderer, G., Emmerling, J., Gernaat, D., Fujimori, S., Strefler, J., Hasegawa, T., Marangoni, G., Krey, V., Kriegler, E., Riahi, K., Van Vuuren, D.P., Doelman, J., Drouet, L., Edmonds, J., Fricko, O., Harmsen, M., Havlík, P., Humpenöder, F., Stehfest, E., Tavoni, M., 2018. Scenarios towards limiting global mean temperature increase below 1.5 C. *Nature Climate Change* 8, 325–332. <https://doi.org/10.1038/s41558-018-0091-3>.
- Ruszczynski, A., 1997. Decomposition methods in stochastic programming. *Mathematical Programming, Series B* 79, 333–353. <https://doi.org/10.1007/BF02614323>.
- Salo, A., Andelmin, J., Oliveira, F., 2022. Decision programming for mixed-integer multi-stage optimization under uncertainty. *European Journal of Operational Research* 299, 550–565. <https://doi.org/10.1016/j.ejor.2021.12.013>.
- Solak, S., Clarke, J.P., Johnson, E., Barnes, E., 2008. A stochastic programming model with decision dependent uncertainty realizations for technology portfolio management, in: *Operations Research Proceedings 2007*, Springer. pp. 75–80. https://doi.org/10.1007/978-3-540-77903-2_12.
- Tarhan, B., Grossmann, I.E., Goel, V., 2009. Stochastic programming approach for the planning of offshore oil or gas field infrastructure under decision-dependent uncertainty. *Industrial and Engineering Chemistry Research* 48, 3078–3097. <https://doi.org/10.1021/ie8013549>.
- Zheng, Q.P., Wang, J., Liu, A.L., 2014. Stochastic optimization for unit commitment—a review. *IEEE Transactions on Power Systems* 30, 1913–1924.
- Zhou, R., Bhuiyan, T.H., Medal, H.R., Sherwin, M.D., Yang, D., 2022. A stochastic programming model with endogenous uncertainty for selecting supplier development programs to proactively mitigate supplier risk. *Omega* 107, 102542. <https://doi.org/10.1016/j.omega.2021.102542>.